This is a preprint of the published article: Zhang, X., Cheng, Y., Dai, S., Li, M., Yuan, Z., & Incecik, A. (2025). A time-domain BEM for instantaneous interaction by two ships head-on encountering in incident waves. Engineering Analysis with Boundary Elements , 172, Article 106128. Advance online publication. https://doi.org/10.1016/j.enganabound.2025.106128

A time-domain BEM for instantaneous interaction by two ships head-on encountering in incident waves

Xiao Zhang[a], Yong Cheng[a,*], Saishuai Dai[b], Mingxin Li[a], Zhiming Yuan[a, b], Atilla Incecik[b]

[a]*School of naval architecture and ocean engineering, Jiangsu University of Science and Technology, Zhenjiang, 212003, China*

[b]*Naval Architecture, Ocean and Marine Engineering Department, University of Strathclyde, Glasgow, United Kingdom*

Abstract: Multi-ship encountering results in complex interactions that significantly modify the surrounding flow field, particularly in the presence of incident waves. Due to the disturbing effect of the complex wave system, the behavior of each ship during the encounter is influenced by the wave characteristics and the relative motions between the ships. This paper establishes a model for ship-to-ship encountering in incident waves using the time-domain Rankine Boundary Element Method (BEM). The transient responses and wave field of ships are investigated. The approach is based on the global fixed system, moment-to-moment iterative updating of the computational grid simulates the two-ship encountering, using the fourth-order Runge-Kutta method for time integration. The classical Wigley III is chosen to calculate and better validate the numerical results for a two-ship encountering in calm water and a single-ship advancing in an incident wave based on the time-domain method. On this basis, a study is carried out to investigate the transient motion and instantaneous wave field of two ships encountering toward an opposite direction in incident waves. Sensitivity analyses of parameters such as wave characteristics, transverse distance between ships, and ship-to-ship speed ratio, reveal that the transient motions of ships are closely related to the incident wave characteristics. Notably, the encounter frequency differs when two ships advance in opposing directions, with variations in transverse distance and speed ratio significantly affecting the amplitude and frequency of their motions during the encounter.

Keywords: hydrodynamic interaction, transient motion, incident wave, encountering operation, wave field, grid update

1. Introduction

Ship-to-ship hydrodynamic interactions have always been one of the trending topics of ocean engineering research. In the open sea, under the action of the wind, waves are created on the surface of the ocean. For a single advancing ship, the presence of incident waves creates a complex wave-ship coupling interaction, where on the one hand the wave forces change the ship motions, and on the other hand, the ship motions affect the surrounding flow field and change the fluid loads. The problem of ship-to-ship advancing in waves is more complicated by the fact that, in addition to the wave action of a single ship, the asymmetric flow generated by the presence of other hulls around it results in lateral actions between ships. This has inspired us to investigate the hydrodynamic effects of ships advancing close together in incident waves, which is also practically significant in ensuring the safety of actual ship navigation.

*Corresponding author: Yong Cheng, mainly research in hydrodynamic performance of floating structures
E-mail: chengyong@just.edu.cn

When the symmetry in the flow field is changed, this change in the flow field affects the navigational safety of ships. To address this problem, scholars have firstly done extensive research on the ship-to-ship hydrodynamic interactions in calm water. Vantorre et al. [1] adopted experimental methods and empirical formulas methods respectively, considered a variety of influencing factors, and simulated the ship-ship interaction forces during the encountering and overtaking process between target vessels. Experimental and empirical formulas methods used to calculate the ship-ship interactions require a large number of experiments to be carried out continuously to determine the results, which consume a lot of materials and time. The continuous development of computer numerical processing techniques has made it easy to use numerical simulation methods to avoid the limitations of the above two approaches. Ohkusu [2], Kodan [3] and Ronæss [4] et al. predicted ship-to-ship hydrodynamic interactions under the two-dimensional slender-body hypothesis, which didn't take into account three-dimensional effects. Later, Korsmeyer et al. [5] considered the influence of 3D effects to study the motions of an arbitrary number of different objects using the 3D panel method. Pinkster [6] extended Korsmeyer's method to calculate the effects of an advancing ship on a moored ship, partially taking into account free surface effects. Yuan et al. [7] accounted for the time term and considered the influence of free surface effects, proposed a reasonable decoupled superposition method accounting for non-constant free surface boundary conditions, and verified its feasibility in predicting hydrodynamic interactions during ships' encounters. This method applies to the problem of an arbitrary object advancing at different speeds in calm water. On this basis, Li et al. [8] used this method to propose a time iterative algorithm containing non-constant nonlinear free surface boundary conditions to investigate the non-constant phenomena of ship-ship interactions in shallow water. In addition, the objects of hydrodynamic research are extensive. For example, Li [9] investigated the drag interference between swimmers, and Yuan et al. [10] used ducks to reveal that multiple waterfowls are able to save individual energy and reduce consumption through formation, and this principle also applies to ships. Future hydrodynamic research is not limited to the ship-to-ship system itself, but also needs to take into account the influence of external factors [11]: the actions of sidewall [12], seabed effects [13], and the coupling of sea waves to the hulls [14] and so on.

On many occasions, due to the influence of sea waves, the above research results of calm water appear to be insufficient or do not reflect the actual phenomena and solve the problems arising in practice. Compared to viscous theory and CFD methods, the methods based on potential flow theory are more computationally efficient and empirically adequate and are still the main methods used for wave-ship coupling analysis. Scholars have done many hydrodynamic responses and drag interference analyses based on the potential flow theory for multiple parallel ships with zero speed and the same speeds in waves. Kashiwagi et al. [15] accurately considered the hydrodynamic interactions of the LNG-FPSO system with a high-order boundary element method within the framework of potential flow theory. Zhu et al. [16] investigated the effects of the gap between multiple floating bodies side-by-side on the hydrodynamic actions and found that the characteristics of the gap have a large effect on the resonant frequency and amplitude of multi-body radiation. Yuan [17] conducted a comparison of the forces and experimental data of a stationary ship with a square box and two parallel ships advancing in waves by the frequency domain Rankine source method and discussed radiation conditions and waveforms in detail. Chen et al. [18] used the time-domain high-order Rankine method to study the motions of side-by-side ships at different separation distances and forward speeds and illustrated that the smaller ships are subjected to fluid forces obviously. Yong and Wen-cai [19] used the frequency domain method to analyze the difference between hydrodynamic interference in waves when three parallel ships and two parallel ships. Li et al. [20] computationally analyzed the hydrodynamic and kinematic responses of two parallel ships advancing in waves using the time-domain Rankine source method and concluded that the numerical method based on the time-domain Rankine source is more flexible than the frequency-domain Rankine source method, and is stable and feasible in calculating the wave-ship coupling.

The time-domain Rankine source method allows for using both free surface kinematics and dynamics conditions in the time step, and only the first-order spatial derivatives need to be included in the problem with forward speed. However, the time-domain Rankine source method has limitations in terms of radiation conditions and needs to prevent the reflection of scattering waves on the boundary of the computational domain during the calculation. He [21] used the time-domain Rankine BEM to achieve the effect of eliminating wave reflections on the free surface boundary during the analysis of waves generated by the Wigley ship and submerged body underway advancing in waves, by adding an artificial damping layer at the boundary of the computational domain. In later related studies, Tang et al. [22], Chen et al. [18], Zhou et al. [23], and Li et al. [20] all carried out relevant hydrodynamic studies on parallel ships in waves by setting up an artificial damping layer.

So far, the hydrodynamic analyses related to wave-ship coupling are mostly based on two or more parallel ships advancing at the same speed in waves, which ignores the change of transient response and free motions of the ships in the whole process. Whereas the process of two ships advancing in opposite directions to each other in waves is all dynamic, the waves generated by one ship act on the other ship, and each ship is subjected to lateral forces given to it by the external waves. Due to advancing in opposite directions, the two ships encounter each other at different frequencies in waves, and they have different flow fields and force effects. On the basis of the study of parallel ships advancing at the same speed [24], and with reference to the computational method of Li's [13] study of the passage of the ship through different seabeds, this paper accounts for the effect of different speeds in the coupled free surface conditions and considers the transient changes when two ships encounter at different speeds.

In this paper, the time-domain Rankine source method is proposed to solve the transient response and hydrodynamic effects of two ships encountering in incident waves. The parts that make up this article are as follows, in section 2, the three-dimensional hydrodynamic theoretical model of ships with speeds under waves in the time domain is illustrated in detail. To ensure the usability of the computational methods in this paper, we have compared the existing models from others in section 3. Section 4 carries out calculations on our research objectives and computationally discusses the impact of relevant factors. Finally, section 5 gives several conclusions.

2. Mathematical statement

2.1. Governing equations and boundary conditions

In this study, two ships are used as a computational model in order to calculate the motions during the encountering in regular waves, two right-handed coordinate systems are displayed in Fig. 1. The coordinate origin o of the fixed reference system $oxyz$ is located on the undisturbed water surface, the x-axis is positive in the direction of incident wave propagation, and the z-axis is vertically upward. The reference coordinate system $o_i x_i y_i z_i$ (i=1, 2) is fixed on each ship advancing with constant speeds U_1 and U_2, respectively, the x_i-axis points toward the bow, and the z_i -axis passes through the center of gravity of the ship vertically upward.

Due to there is a speed, the fixed coordinate system and the reference coordinate system no longer coincide, and the calculation of the motions and forces of each ship is carried out in the reference coordinate system, and the conversion relationship between the fixed coordinate system and the reference coordinate system is as follows:

$$(x, y, z) = (x_i + U_i t, y_i, z_i), \quad i=1,2 \tag{1}$$

The fluid is assumed to be an incompressible, inviscid ideal fluid with irrotational motion and water depth is d. The incident wave is assumed to be a micro-amplitude wave with an incident frequency ω_0, and the wave number k determined by the dispersion relation:

$$k = \omega_0^2 / g \tanh(kd). \tag{2}$$

Since two ships are advancing at different speeds, they are subjected to different wave encounter frequencies, which in the reference coordinate system can be given by

$$\omega_{e,i} = \omega_0 - kU_i \cos\beta, \quad i = 1, 2 \tag{3}$$

in which β is the incident wave angle.

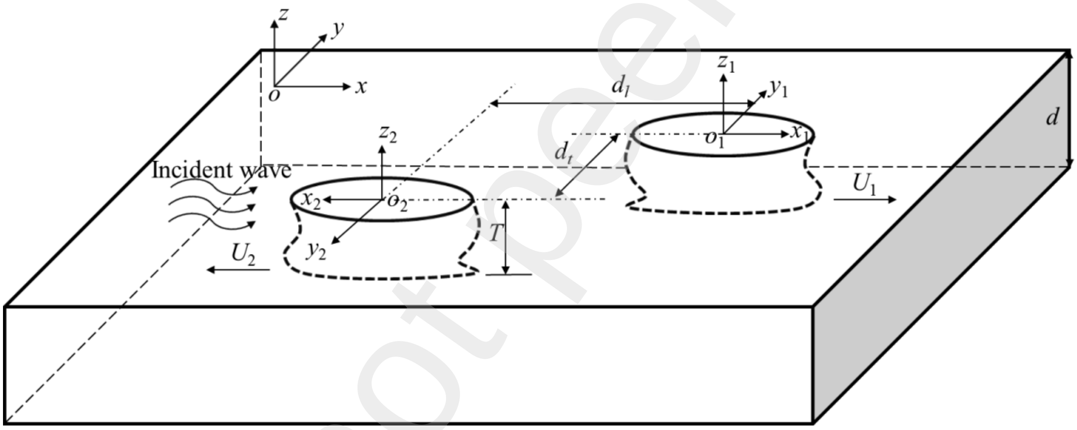

Fig. 1. Sketch of coordinate system.

In the framework of linear potential flow theory, the total velocity potential within the whole flow field is expressed as Φ in the reference coordinate system satisfies the Laplace equation.

$$\nabla^2 \Phi = 0, \tag{4}$$

For the treatment of problems where different velocities exist, the total velocity potential Φ is a coupled superposition of the individual velocity potentials of each ship in the flow field,

$$\Phi = \sum_{i=1}^{N} \Phi_i = \sum_{i=1}^{N} \phi_i^s + \phi_i^I + \phi_i^D, \tag{5}$$

in the above equation, N is the number of ships, there N=2, ϕ_i^S is the steady-disturbance flow caused by the ship's wash waves, ϕ_i^I is the incident potential, and ϕ_i^D is the non-constant disturbed potential caused by the waves. Among them, the incident potential ϕ_i^I has an analytical solution, and its defining equation is expressed as:

$$\phi_i^I(x_i, y_i, z_i, t) = \frac{gA}{\omega_0}\frac{\cosh k(z_i+d)}{\cosh kd}\sin[k(x_i\cos\beta + y_i\sin\beta) - \omega_{e,i}t], \quad (6)$$

where g is gravitational acceleration, A is the amplitude of the incident wave, d is water depth.

The non-constant disturbed potential ϕ_i^D consists of the diffraction potential ϕ_i^d and the radiation potential ϕ_i^r, i.e. $\phi_i^D = \phi_i^d + \phi_i^r$.

When the velocity potential Φ_i is known, the hydrodynamic force on the ship body i in its own coordinate system can be found from Bernoulli's equation and then integrated:

$$\begin{aligned} & p_i = \rho\left(\boldsymbol{U}_i\frac{\partial \Phi_i}{\partial x_i} - \frac{\partial \Phi_i}{\partial t}\right) \\ & F_i^j = \iint_{S_i} p_i n_i^j dS_i \end{aligned}, \quad i = 1, 2,\ j = 1, 2, 3, 4, 5, 6 \quad (7)$$

where S_i is the i-th wetted ship body surface, j represents six degrees of freedom include surge, sway, heave, roll, pitch and yaw.

In order to make the solution of the velocity potential satisfy the Laplace equation Φ_i unique, it is also necessary to give the corresponding boundary conditions.

In this paper, ship 1 and ship 2 have different advancing speeds, which satisfies the conditions of the decoupled superposition method in Yuan et al. [7]: ship 1 and ship 2 satisfy the velocity potentials ϕ_1^s and ϕ_2^s, respectively, that arise when one of them is advancing while the other is stationary. The details are as follows:

$$\begin{cases} \nabla^2 \phi_1^s = 0 & \\ \boldsymbol{U}_1^2 \dfrac{\partial^2 \phi_1^s}{\partial x_1^2} + g\dfrac{\partial \phi_1^s}{\partial z_1} = 0 & \text{on } z = 0 \\ \dfrac{\partial \phi_1^s}{\partial n_1} = \boldsymbol{U}_1 n_1^1 & \text{on ship 1} \\ \dfrac{\partial \phi_1^s}{\partial n_2} = 0 & \text{on ship 2} \\ \dfrac{\partial \phi_1^s}{\partial z} = 0 & \text{on } z = -d \end{cases} \quad (8)$$

and

$$\begin{cases} \nabla^2 \phi_2^s = 0 & \\ \boldsymbol{U}_2^2 \dfrac{\partial^2 \phi_2^s}{\partial x_2^2} + g\dfrac{\partial \phi_2^s}{\partial z_2} = 0 & \text{on } z = 0 \\ \dfrac{\partial \phi_2^s}{\partial n_1} = 0 & \text{on ship 1} \\ \dfrac{\partial \phi_2^s}{\partial n_2} = \boldsymbol{U}_2 n_2^1 & \text{on ship 2} \\ \dfrac{\partial \phi_2^s}{\partial z} = 0 & \text{on } z = -d \end{cases} \quad (9)$$

In the above equation, $\boldsymbol{n}_i$ is denoted as the normal vector of the wet surface of ship i, defined as

$(n_i^1, n_i^2, n_i^3) = \boldsymbol{n_i}$, $(n_i^4, n_i^5, n_i^6) = \boldsymbol{r_i} \times \boldsymbol{n_i}$, with $\boldsymbol{r_i}$ being the direction vector of the field point of the wet surface of ship i pointing towards the center of gravity of the ship.

The rocking motion of a ship in waves is mainly related to $\phi_\mathrm{i}^I, \phi_\mathrm{i}^d, \phi_\mathrm{i}^r$. The non-constant diffraction potential ϕ^d is also decoupled in such a way (Eq.(8) and (9)), so the object plane condition can be decoupled as $\phi_1^d$and ϕ_2^d:

$$\begin{cases} \dfrac{\partial \phi_1^d}{\partial n_1} = -\dfrac{\partial \phi_1^I}{\partial n_1} & \text{on ship 1} \\ \dfrac{\partial \phi_1^d}{\partial n_2} = 0 & \text{on ship 2} \end{cases} \tag{10}$$

and

$$\begin{cases} \dfrac{\partial \phi_2^d}{\partial n_1} = 0 & \text{on ship 1} \\ \dfrac{\partial \phi_2^d}{\partial n_2} = -\dfrac{\partial \phi_2^I}{\partial n_2} & \text{on ship 2} \end{cases} \tag{11}$$

The radiation problem of two ships in waves is much more complicated than that of a single ship, which is due to the fact that the simple harmonic vibration of each ship is the result of the combined action of each wave on its hull, and thus its radiation problem is coupled [20]. Extending this principle to the case of two ships with different speeds encountering in this paper, each ship body surface condition for the radiation potential ϕ_i^r can be simplified as

$$\frac{\partial \phi_i^r}{\partial n_i} = \sum_{j=1}^{6} \left(\frac{\partial \xi_i^j}{\partial t} n_i^j + \boldsymbol{U}_i \xi_i^j m_i^j\right), \qquad i = 1,2 \tag{12}$$

in the above equation, ξ_i^j denotes the displacement of ship i in the j-th direction of motion, and m_i represents the coupling between the steady flow and the non-constant flow

$$\begin{cases} (m_i^1, m_i^2, m_i^3) = -(\boldsymbol{n}_i \cdot \nabla)\nabla \phi_i^s \\ (m_i^4, m_i^5, m_i^6) = -(\boldsymbol{n}_i \cdot \nabla)(\boldsymbol{r}_i \times \nabla \phi_i^s) \end{cases}. \quad i = 1,2 \tag{13}$$

In this study, it is assumed that the ship is a slender body, the simplified m_i term using Neumann-Kelvin linearization is

$$\begin{cases} (m_i^1, m_i^2, m_i^3) = (0,0,0) \\ (m_i^4, m_i^5, m_i^6) = (0, n_i^3, -n_i^2) \end{cases}. \quad i = 1,2 \tag{14}$$

The non-constant disturbed potential ϕ_i^D satisfies the linear kinematic and dynamic boundary conditions at the free surface with z =0, respectively, and neglects the second-order terms. Additionally, in order to satisfy the radiation condition, a numerical damping layer is required to be installed in both the linear kinematic and dynamic boundary conditions, to avoid wave reflection at the end of the finite computational domain. Then the free surface conditions are written as:

$$\begin{cases} \dfrac{\partial \phi_i^D}{\partial t} = -g\zeta_i^D - \nu(r)\phi_i^D \\ \dfrac{\partial \zeta_i^D}{\partial t} = \dfrac{\partial \phi_i^D}{\partial z_i} - \nu(r)\zeta_i^D \end{cases}, \quad i = 1,2 \tag{15}$$

where $\nu(r)=\begin{cases}\alpha_0\omega_0\left(\dfrac{r-r_0}{\beta_0\lambda}\right)^2 & r_0\le r\le r_1=r_0+\beta_0\lambda\\ 0 & r<r_0\end{cases}$ (16)

is the damping layer coefficient. It is determined by the damping layer coefficient α_0, and the thickness of the damping layer $\beta_0\lambda$, λ is the incident wavelength, r_0 is the start of the damping layer, is the length of the computational domain. And the initial conditions are met: $\phi_i^D|_{t=0}=0$, $\frac{\partial\phi_i^D}{\partial n_i}|_{t=0}=0$.

2.2. Numerical methods

2.2.1. Boundary integral equation

After satisfying the Laplace equation and determining the boundary conditions, the three-dimensional problem is transformed into a two-dimensional problem for solving the velocity potential through Green's theorem. In this paper, the boundary element (BEM) method is used to obtain the boundary integral equation satisfied by the velocity potential in the domains through Green's second theorem:

$$\phi(P_i)=\iint_S\sigma(Q_i)G(P_i,Q_i)ds,\qquad i=1,2 \tag{17}$$

where ϕ can be replaced by ϕ_i^s or ϕ_i^D, $P_i(x_i, y_i, z_i)$ denotes the field points, $Q_i(\xi_i, \eta_i, \zeta_i)$ denotes the source points. $\sigma(Q_i)$ is the source distribution density on the wet surface of the hull, $G(P_i, Q_i)$ is the Rankine source function, i.e. $G\left(P_i,Q_i\right)=\frac{1}{r_i}+\frac{1}{r_i'}$, which is distributed uniformly on the object surface as well as on the free surface, $r_i=\sqrt{(x_i-\xi_i)^2+(y_i-\eta_i)^2+(z_i-\zeta_i)^2}$ is the distance between the field point P_i and the source point Q_i, and $r_i=\sqrt{(x_i-\xi_i)^2+(y_i-\eta_i)^2+(z_i+\zeta_i+2d)^2}$ is the distance between the field point P_i and the mirror-image source point Q_i.

In order to solve the boundary integral equation, the computational wet boundary S is dispersed into small surface elements including body elements S_B and free surface S_f by using the quadrilateral surface element method, i.e. $S=\sum NB\ jS_B+\sum NF\ jS_f$, j is the number of computational panels. The velocity potential of the source point on each surface element is considered to be a constant, and the integral form of the velocity potential at the field point P_i can be expressed as

$$\phi(P_i)=\iint_{\sum_{j=1}^{NB}S_B+\sum_{j=1}^{NF}S_f}\sigma(Q_i)G(P_i,Q_i)ds=\sum_j^S\sigma_jG_{i,j}.\quad i,\ j=1,2,...,N \tag{18}$$

The influence coefficients $G_{i,j}$ can be derived analytically, and the matrix form of the boundary integral equation is obtained by substituting the above equation into the boundary conditions satisfied by each velocity potential:

$$A_{i,j}q_j=B_j, \tag{19}$$

where i and j are from 1 to S, S denotes the total number of surface elements and A_{ij} is the matrix of influence coefficients. After that, the source strength distribution density $\sigma(Q_i)$ corresponding to each velocity potential on each ship surface is solved by the LU decomposition method, and the obtained source strength distribution density $\sigma(Q_i)$ is brought into the above equation that is determined to obtain the required velocity potential ϕ.

2.2.2. Equations of motion

Considering the ship body as a rigid body, which is subject to inertial and repulsive forces in addition to satisfying the wave forces, and according to Newton's second law, the following differential equations of motion with six degrees of freedom for each hull can be derived:

$$M_i\left\{\ddot{\xi}_i^j\right\}+B_i\left\{\dot{\xi}_i^j\right\}+C_i\left\{\xi_i^j\right\}=F_i^j, \qquad i=1,2,\ j=1,2,3,4,5,6 \tag{20}$$

where M_i, B_i and C_i are the mass matrix, the viscous damping matrix and the response moment array of two ships, respectively, both of which are 6×6 matrices; ξ_i^j, $\dot{\xi}_i^j$ and $\ddot{\xi}_i^j$ are the kinematic displacements, velocities and accelerations of the i-th ship under the action of the wave, respectively; and F_i^j denotes the wave excitation forces and moments on the i-th ship. The j denotes the six degrees of freedom of the motion response of each ship body.

For numerical stability and accuracy, the equations of motion is solved by the fourth-order Runge-Kutta method, which is computed in four iterations with Δt as the time increment at each moment t. The acceleration $\ddot{\xi}_{i,k}^{j,t}$ (k=1, 2, 3,4, represents the number of iterations of Δt) is obtained at every time step of the i-th ship body, respectively, then the motion $\xi_i^{j,t+1}$ and $\dot{\xi}_i^{j,t+1}$at the new moment t+1 are got:

$$\begin{aligned}\xi_i^{j,t+1}&=\xi_i^{j,t}+\Delta t\cdot\dot{\xi}_i^{j,t}+\Delta t\cdot\frac{(\ddot{\xi}_{i1}^{j,t}+\ddot{\xi}_{i2}^{j,t}+\ddot{\xi}_{i3}^{j,t})}{6}\\ \dot{\xi}_i^{j,t+1}&=\dot{\xi}_i^{j,t}+\frac{(\ddot{\xi}_{i1}^{j,t}+2\ddot{\xi}_{i2}^{j,t}+2\ddot{\xi}_{i3}^{j,t}+\ddot{\xi}_{i4}^{j,t})}{6}\end{aligned}, \ i=1,2,\ j=1,2,3,4,5,6 \tag{21}$$

and the cycle is repeated until the end of time.

2.2.3. Free surface update

The free-surface kinematic and dynamic boundary conditions involve time terms, and for each ship body, the fourth-order Runge-Kutta method of iterative time advancement scheme is similarly adopted to update the non-constant disturbed velocity potential ϕ_i^D and the free surface elevation ζ_i^D:

$$\begin{aligned}\phi_i^{D,t+1}&=\phi_i^{D,t}+\Delta t\cdot\frac{(\phi_{i1}^{D,t}+2\phi_{i2}^{D,t}+2\phi_{i3}^{D,t}+\phi_{i4}^{D,t})}{6}\\ \zeta_i^{D,t+1}&=\zeta_i^{D,t}+\Delta t\cdot\frac{(\zeta_{i1}^{D,t}+2\zeta_{i2}^{D,t}+2\zeta_{i3}^{D,t}+\zeta_{i4}^{D,t})}{6}\end{aligned}. \quad i=1,2 \tag{22}$$

3. Numerical validation

Prior to the present analytical study, the mesh convergence and time step convergence test are carried out, after which this paper verifies the computational validity of the involved two-ship encountering in calm water and the single-ship model advancing in head waves using the time-domain Rankine source method, respectively, to confirm the usability of the present method. So a combination of these two motion modeling methods is used to apply to the behavioral study of two-ship encountering in waves in the next section.

Parameter	Value
Length (*L*)	3m
Breath (*B*)	0.3m
Draft (*T*)	0.1875m
Water depth (*d*)	1.3125m
Transverse distance between ships (*dt*)	0.6m

Table 1 Relevant parameters for calculations.

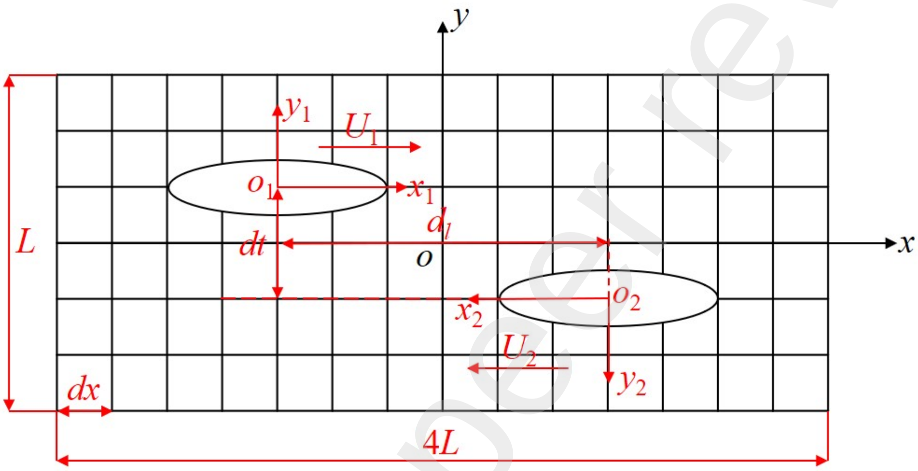

Fig. 2. Mesh distribution of two Wigley III ships advancing in opposite directions in calm water.

3.1. Convergence test

Since the ship-to-ship encountering problem requires ships to be stepped over time, a convergence study of both the mesh and the time step is required. Wigley III is selected as the model for the study, and the model dimensions and the sketch of ship-to-ship encountering are shown in Table 1 and Fig. 2, respectively. The hydrodynamics are uniformly dimensionless as:

$$C_Y = \frac{F_Y}{0.5\rho |U_1 U_2| BT}$$
$$C_{ZZ} = \frac{F_Z}{0.5\rho |U_1 U_2| BTL}, \tag{23}$$

where ρ is the density; U_1, U_2 are the ships' speeds and depend on $Fn\sqrt{gL}$, here Fn = 0.2 is the same as the validation parameter in the next section; F_Y, F_Z are the sway force and the yaw moment, respectively.

3.1.1. Mesh Convergence

In the 3.1.1 and 3.1.2 sections, the rigid-wall free-surface condition ($\frac{\partial \phi}{\partial z} = 0$) is used to simplify the model so that convergence can be observed more easily.

The mesh convergence study is divided into three meshes, with mesh cell length (see Fig. 2) $dx=L/60$ (fine mesh), $dx=L/30$ (standard mesh) and $dx=L/20$ (coarse mesh). The hydrodynamic comparisons of two ships encountering in calm water under the three meshes are shown in Fig. 3, and the results of the ship-ship interaction forces in calm water under $dx=L/60$ and $dx=L/30$ are very similar and better than $dx=L/20$. Therefore, for the convenience of saving computational time on the meshes, the standard mesh ($dx=L/30$) can achieve the computational results.

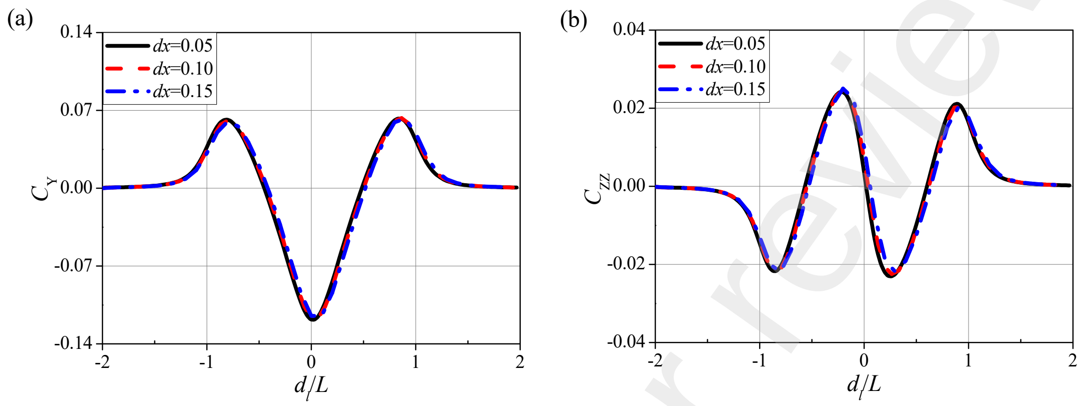

Fig. 3. Mesh convergence. (a) Sway force; (b) yaw moment.

3.1.2. Time step convergence

Since each time step is required for the ship-ship encountering, and the time step is related to the mesh size, and the size of the time step needs to coincide with the mesh size, a convergence study is performed for the time step. The time step is set as $\Delta t=dx/2U$, $\Delta t=dx/U$ and $\Delta t=2dx/U$ (dx is the mesh length, U is the speed), respectively. The results for all time steps are shown in Fig. 4. In the calculations it is necessary to ensure that the data information generated by the ship moving through one time step can be captured and the time step should not be too large. The calculations show that $\Delta t=dx/U$ is sufficiently feasible and more computationally time efficient compared to $\Delta t=dx/2U$, which means that the ship moves one grid distance for each time step.

So the standard mesh ($dx=L/30$) and $\Delta t=dx/U$ are chosen to be applied in the following calculations.

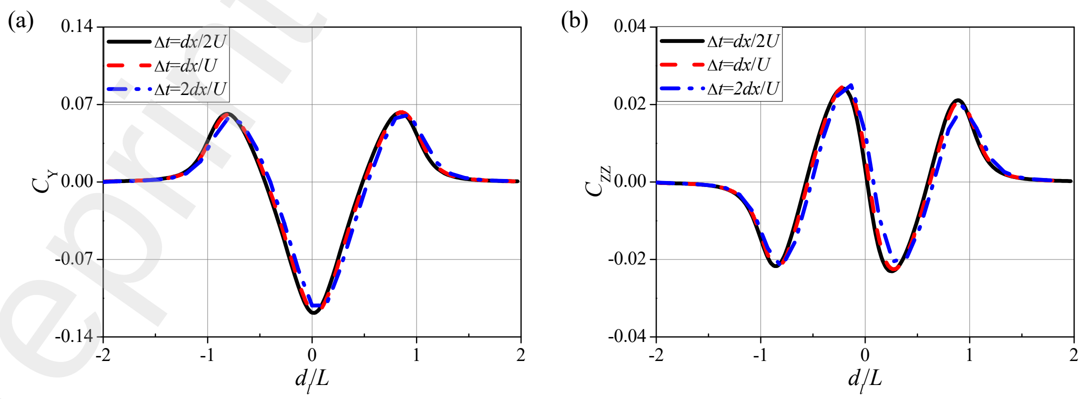

Fig. 4. Time step convergence. (a) Sway force; (b) yaw moment.

3.2. Validation test

3.2.1. Two ships advancing in opposite directions in calm water

The computational sketch and parameters for two Wigley III ships encountering in calm water are shown in Fig. 2 and Table 1, with two ships at transverse distance dt (dt= 0.6m) advancing toward an opposite direction at a speed of Fn = 0.2, respectively. In this calculation, a decoupled superposition method is used, where the encounter process problem is considered as two steady-state problems and free surface effects are considered (Eq.(8) and(9)). The hydrodynamic forces obtained from Eq. (23) is compared with the results of Yuan et al. [7] (see Fig. 5). Generally, there is good agreement between calculations.

It is obvious from Fig. 5 and Fig. 6 that two ships interact as soon as they meet at the bow, and the attraction between two ships is greatest when d_l/L=0 and transfers from the near field to the far field as the ships move (d_l/L <0), with the far-field wave disturbance producing a much larger and unpredictable effect. In summary, the hydrodynamic changes are evident during the bow encounter and stern departure phases, and these two positions are subject to both lateral forces and yaw moments when they are just about to make contact.

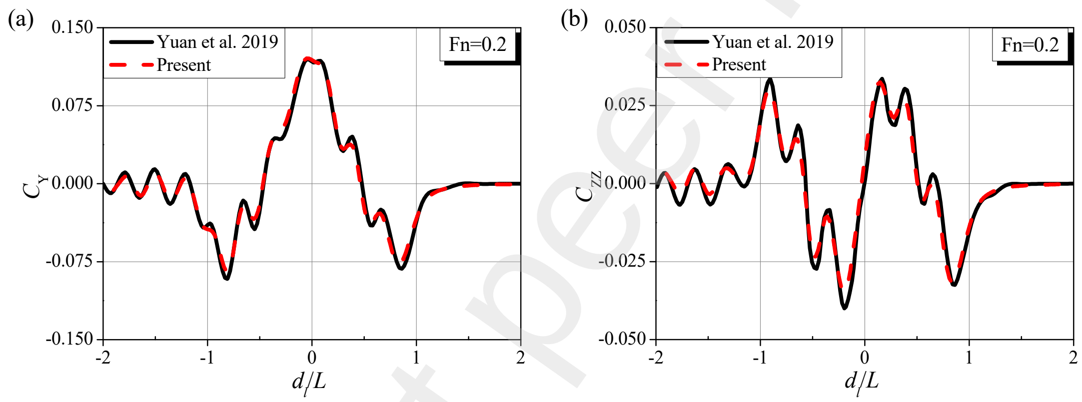

Fig. 5. Sway forces on two Wigley III ships encountering in calm water at a transverse distance dt=0.6m. (a) Sway force; (b) yaw moment. The horizontal coordinates indicate the longitudinal distance between two ships, d_l/L =0 indicates alignment in ships, d_l/L >0 indicates before the encounter, and d_l/L <0 indicates after the encounter.

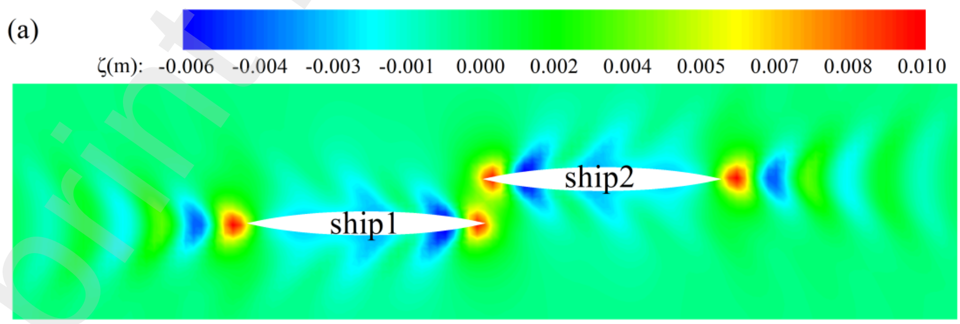

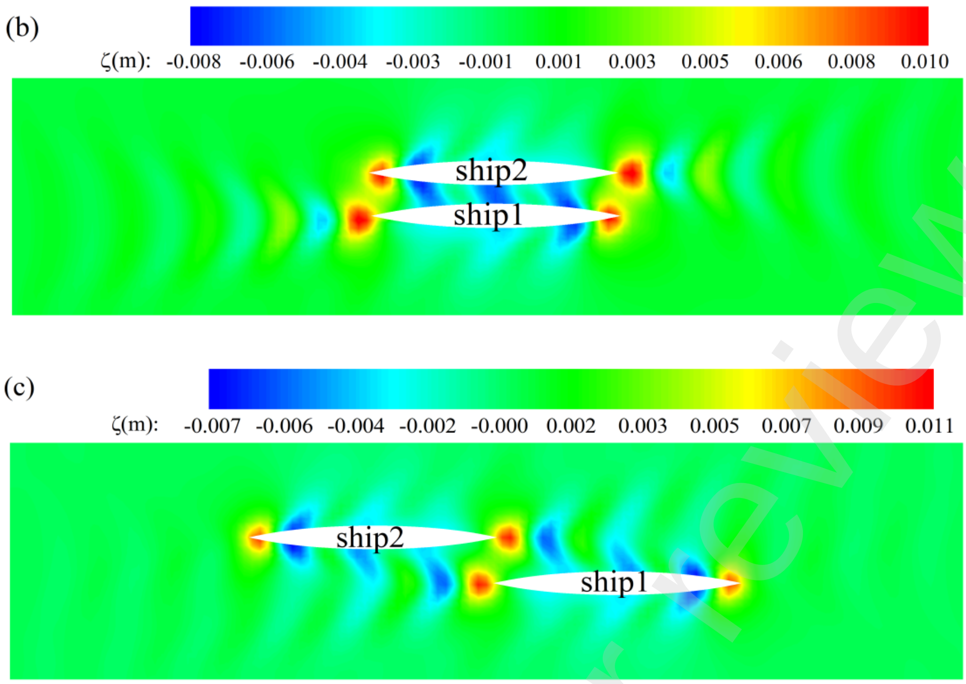

Fig. 6. Wave patterns of two Wigley III ships during the encounter at $F_n = 0.2$. (a) d_l/L=1; (b) d_l/L=0; (c) d_l/L=-1.

3.2.2. Single ship in incident waves

The detailed description of the computational domain is shown in Fig. 7: the single Wigley III advancing in head waves (wave amplitude $\xi_0 = 0.05$m, wave direction β =180°) at Fn = 0.2. Other parameters are as in Table 1. The free surface of the entire computational domain covers a length of 6L in the x-axis direction and 2.4L in the y-axis.

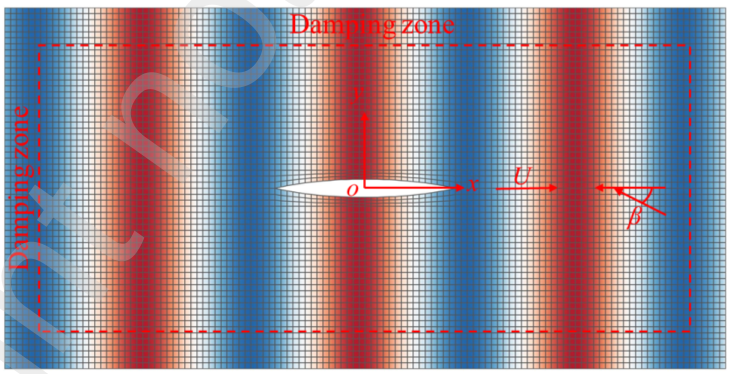

Fig. 7. Meshing grid. The entire computational domain including the hull section is divided into 13560 panels for computation.

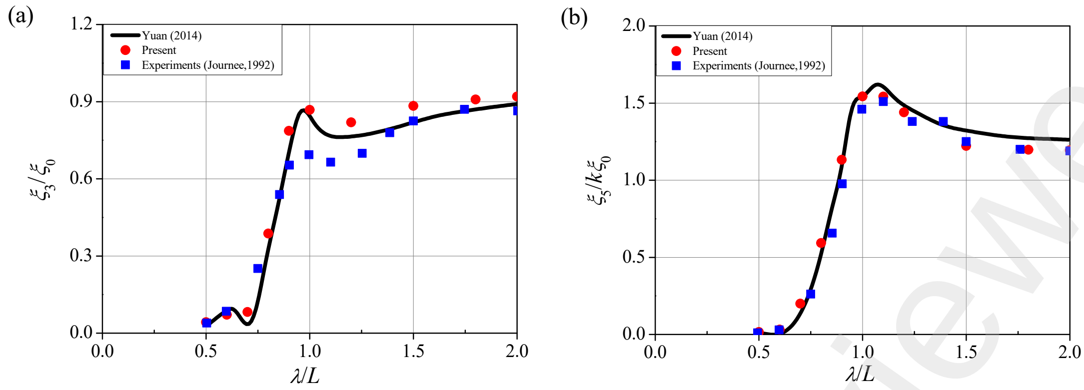

Fig. 8. Ship motion response amplitudes for Fn=0.2. (a) Heave response;(b) pitch response. The horizontal coordinate is the dimensionless wavelength, λ is the wavelength.

The comparison of the motion response at different wavelengths is shown in Fig. 8. The results of the present calculations are consistent with the trend of changes in Yuan [17] and Journee [25]. The problem of a single ship advancing in incident waves has been studied a lot and solved based on the ship's own coordinate system, for which an extra convection term is added to the computation. However, in this paper, considering that the ships encounter in incident waves is a dynamic problem, based on the global coordinate system reference, the ships constantly change their positions, while ignoring the convection term. In addition, the velocity potential in the frequency-domain joint free-surface condition used in Yuan [17] contains a second-order term, whereas the time-domain Rankine method used in this paper applies both the kinematic and dynamic conditions on the free surface, so that only the first-order spatial derivatives are included, and this subtle difference results in a few slightly different data points in the long wave, but no difference in the short wave. Therefore, it is acceptable to have some numerical discrepancies in Fig. 8.

4. Results and discussion

Based on section 3, this section will investigate the problem of motion interference between two Wigley III ships encountering toward an opposite direction in incident waves using the time-domain Rankine source method. Furthermore, factors affecting interference between ships are computationally analyzed, including the incident wave characteristics, the transverse distance between ships, and the velocity ratio between ships.

4.1. Ship-to-ship transient response in regular waves

During this study, assuming that the incident wave is a micro-amplitude wave, the motions of both ships in Fig. 9 are constrained by the direction of the sway, surge and yaw, while the heave, roll and pitch are free. At the end of each computational moment, the free-surface mesh is updated and the velocity potential is calculated with the iterative updating of the free surface, the wave elevation and velocity potential values for the next moment are predicted using two-dimensional interpolation, so that it can approximate the free surface at the next time step. This results in the influence matrix changing at each moment, which increases the computation time. The grid distribution of the computational domain and the two Wigley III ships is shown in Fig. 10, with 12960 panels on the computational domain and 1200 panels on the two ships.

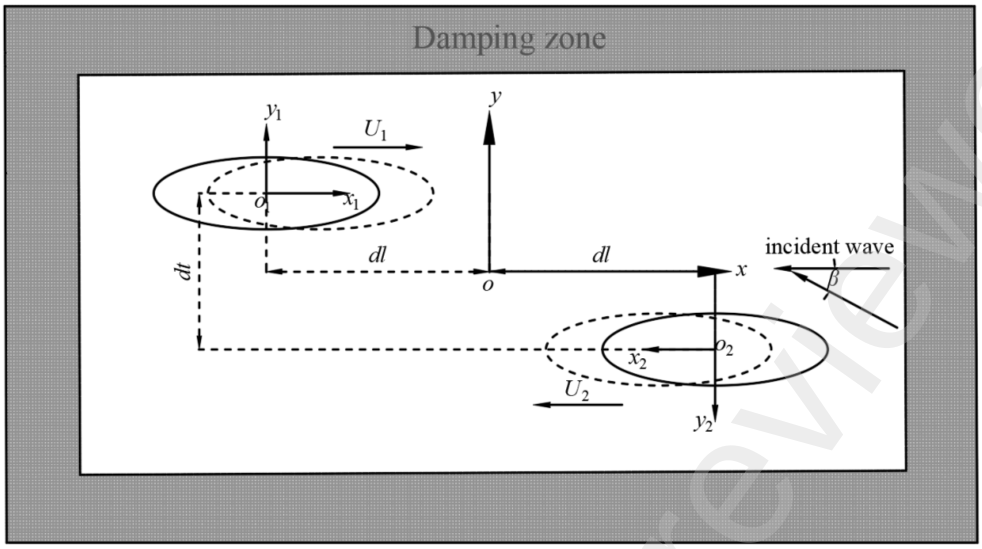

Fig. 9. Sketch of two ships encountering in incident waves.

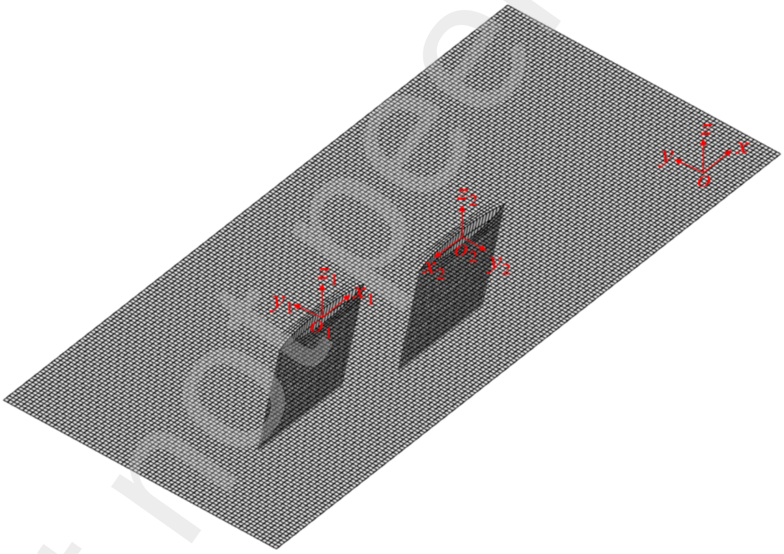

Fig. 10. Grid distribution of the computational domain.

Two ships initially separated by 2*dl* (if not specified, *dl* = 6m) advance anisotropically in the head wave (β=180°) at a speed of Fn=0.2 respectively, the transverse distance between two ships is *dt* (*dt*=0.6m). For a single Wigley III ship, the resonance frequency of the heave and pitch motions are that when wavelength λ/L is between 1.0 and 1.2m [20]. The incident wave height ξ_0=0.05m and the wavelength is chosen to be λ=3m. In order to avoid initial effects during the calculation, the incident potential is multiplied by a ramp function allowing the scattering potential to develop gradually, as in Eq.(24), where T_m is the wave period that satisfies $T_m = 2\pi/\omega_0$. Fig. 11 shows the non-dimensional amplitudes of heave and pitch motions of two ships in the model of this study advancing individually in the corresponding waves (ship 1 in head waves, ship 2 in following waves) and compared with the motions of two ships encountering. The changes in motions that occur when two ships meet (*t*=4.1s ~6.9s) are observed.

$$F_m = \begin{cases} 0.5\left[1-\cos(\frac{\pi t}{T_m})\right] & t < T_m \\ 1 & t \geq T_m \end{cases} \quad (24)$$

Two ships advancing in opposite directions in an incident wave are subjected to different encounter frequency ω_e, resulting in different Brard numbers τ for two ships ($\tau = U\omega_e/g$, $\tau_1 > 0.25 > \tau_2$), and different sailing waveforms for ship 1 and ship 2. The difference in dynamic motions between ship 1 and ship 2 is apparent in Fig. 12. Ship 1 advances in the head waves, its speed is slower compared to the incident waves, so it encounters more waves per unit of time. While ship 2 advancing in the following waves, the thrust of the waves makes the ship faster than the waves. These cause the two ships to have different cycles of motion. The heave and pitch motions of two ships without the encounter and after the encounter are consistent with the motions of a single ship advancing under the same conditions (see Fig. 11). Ship 1 advancing in head waves produces more significant heave and pitch motions, while ship 2 advancing in the following waves is subjected to less heave and pitch motions. Two bows begin to meet at t=4.1s and the sterns move away from each other at about t=6.9s. During this period, the motion responses are complicated by the fact that the ship wash waves generated by each ship touch the other ship and reflect back. Whereas two ships have been advancing forward, the reflected waves act on different parts of the hulls to cause transient effects, increasing the instability of the motions and complicating the motion responses. Waves spreading from the bow to the stern in the direction of ship 2 advancing have little effect on the heave and pitch motions of ship 1, ship 2 is significantly affected by divergent waves from ship 1, which produced significant instability changes in the amplitude as well as the waveform over time (see Fig. 12(a)-(c)).

The single ship hardly produces lateral motion when advancing in waves, while two-ship advancing produces a roll motion due to the ship-to-ship interactions causing pressure differences between the ports and starboards of ships, as shown in Fig. 13, diffracted and radiated wave components are mainly captured in the gap between two ships, constituting a lateral interference and thus generating the roll motions, Fig. 12(b) shows the changes in roll motions when two ships are advancing in opposite directions. After two bows meeting, ship 1 is subjected to much less roll motions compared to ship 2, and the values of the motions are not of the same order of magnitude. It should be noted that when the bow of ship 2 touches the action of the wash wave of ship 1, the amplitude of motion changes sharply during the encounter, ship 2 is more unstable than ship 1. After the encounter, the heave and pitch of the two ships gradually stabilize, and the roll motion of ship 1 begins to decay, while ship 2 is still subject to the roll motions under the combined effects of the scattered and transmitted from ship 1 to ship 2 (e.g. Fig. 14). Overall, in the same sea state, the ship advancing in following waves is more easily to external disturbances and generates instability and the ship in head waves is more stable and subject to less lateral action. The drastic changes in motion between two ships have an important effect on the maneuverability and stability of ships.

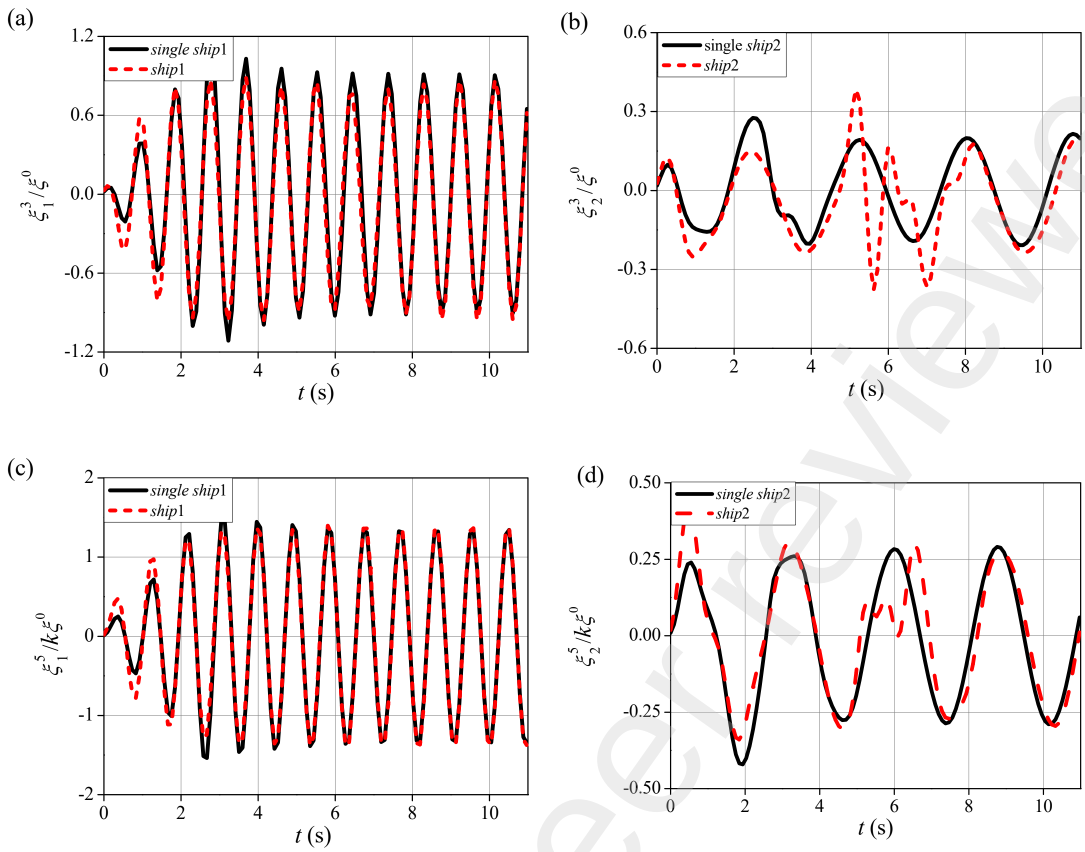

Fig. 11. Time series of the motion response of two ships at Fn = 0.2 with the corresponding ships in two-ships encountering respectively. (a) Heave motions on ship 1; (b) heave motions on ship 2; (c) pitch motions on ship 1; (d) pitch motion on ship 2.

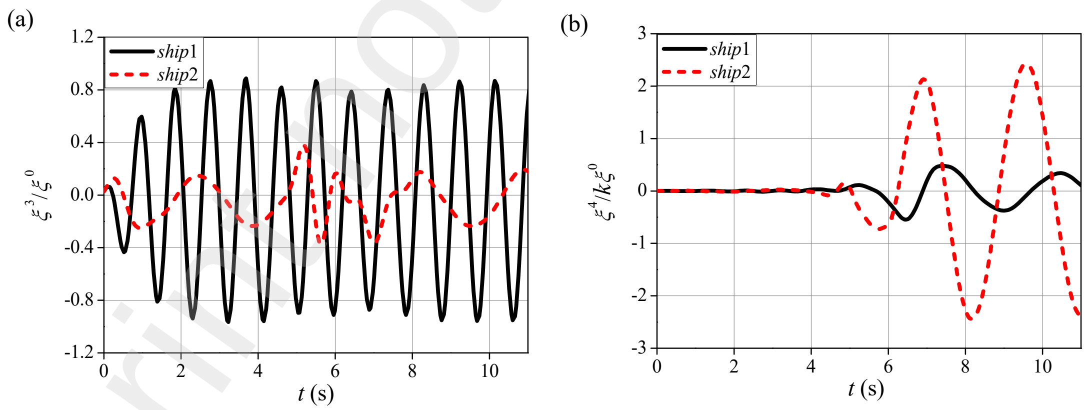

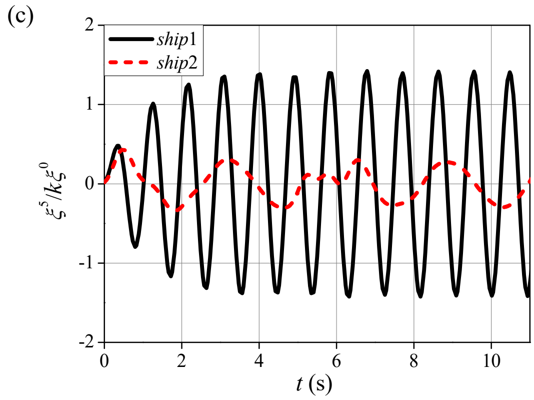

Fig. 12. Time series of the motion response of two ships advancing during the encounter process. (a) Heave motion; (b) roll motion; (c) pitch motion.

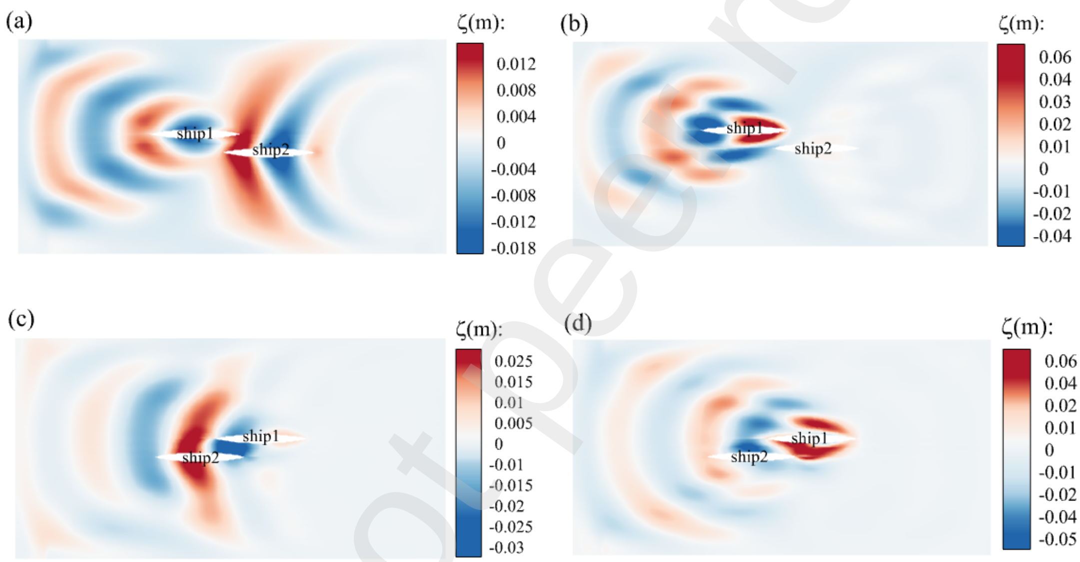

Fig. 13. Wave elevation of two ships with the speed in head sea (λ=3m, Fn=0.2, dt=0.6m). (a) Diffracted wave of the bow encounter; (b) radiated wave of the bow encounter; (c) diffracted wave of the stern encounter and (d) radiated wave of the stern encounter.

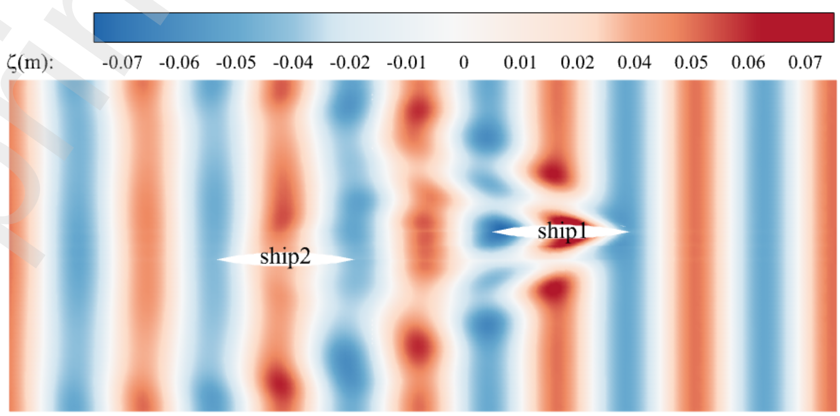

Fig. 14. Wave patterns after the encounter (t=8.3s).

4.2. *Effects of incident wave direction on transient motions*

From the encounter frequency of Eq.(3), it is clear that the motions of the advancing ship in incident waves are closely related to the incident wave direction angle β. The case of longitudinal incident waves (β=180°) has been investigated previously, when the incident wave is perpendicular to the ship (β=90°) and close to the wake (β=150°), the roll and pitch motions are more pronounced, respectively, allowing an assessment of the ship's motion in the most unfavorable case.

Fig. 15 displays the instantaneous motion variations of two ships for two oblique wave conditions at an initial distance ($2dl$ = 10m). In addition to the effect of scattered and reflected waves, the two ships also have the effect of oblique waves on their roll motions, which makes the roll motions more significant compared to β=180°. When β =90°, the transient motions of ship 1 and ship 2 are approximately the same. At λ=3, the amplitude of the heave motion β =90° is closer to 1.0 than the amplitude of the 180°, because the frequency in this case is close to the resonance frequency. Additionally, it is worth noting that the roll variations of two ships in Fig. 15(c) and (d) have two positive amplitudes in one variation period, which may be due to the reflected wave effect on the beginning of the bow-to-bow encounter of two ships at $t \approx$ 3s. When β shifts from 90° to 150°, the encounter frequency ω_e of both ships changes, the transient effects of the motions become more obvious, and the motions are in an unsteady state during the encounter (t=3~6s), and the frequency of the respective motions change. For ship 1, the roll motion at β = 150° is smaller than the motion for the β = 90° case due to the reduced wave component in the y-direction, while ship 2 has a larger roll motion. In the vertical direction, the amplitudes of heave motions decrease for both ships, whereas for the longitudinal motion, the angles between the incident wave direction and the heading of two ships are changed, resulting in the waves impacting the bow of ship 1 and the stern of ship 2, respectively, and generating a larger impact on the longitudinal direction of ships, the pitch motion amplitudes of two ships increase and the frequency of the pitch motion of ship 2 is significantly changed with a greater preference for the following direction, the amplitudes tend to be stable around 0.3 after the encounter.

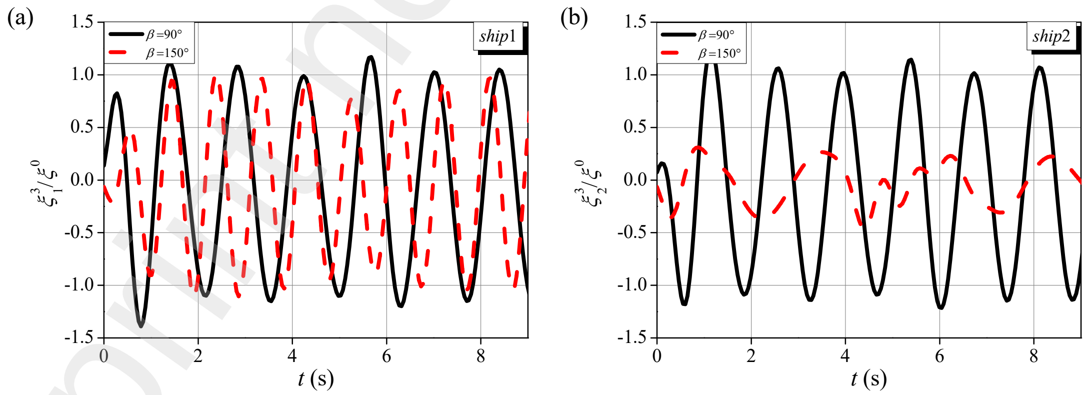

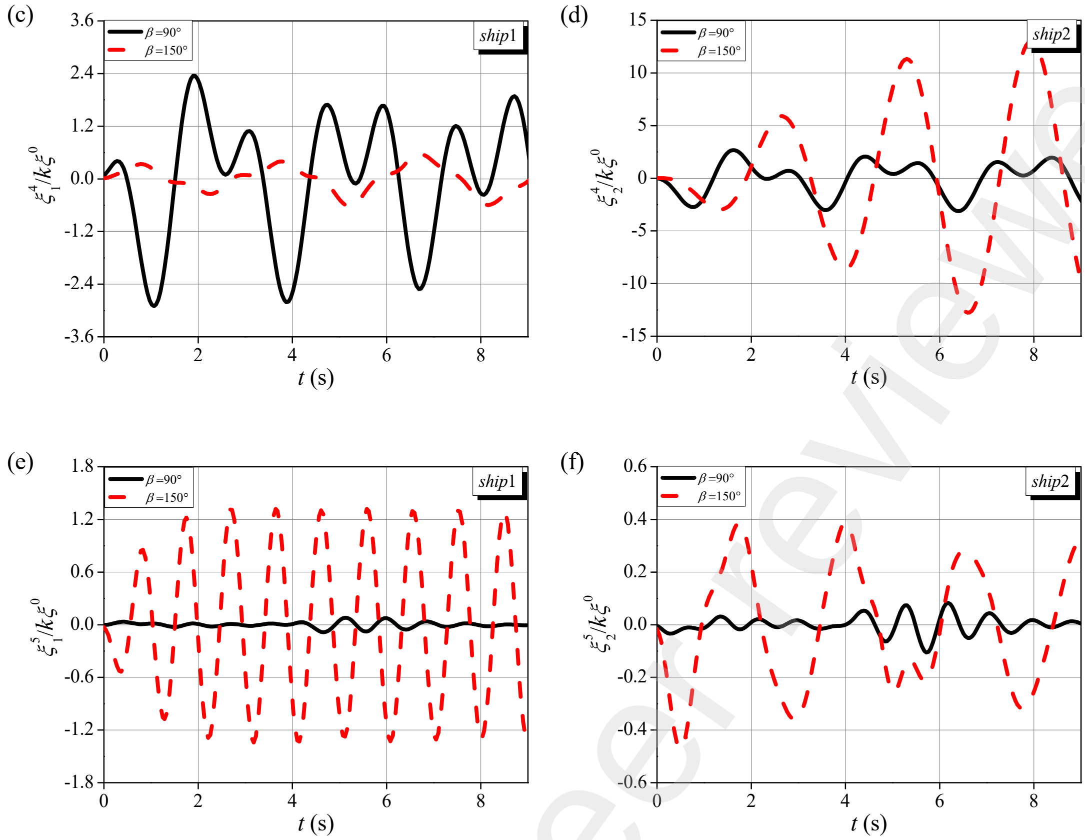

Fig. 15. Time series of two ships' motions with different incident wave angles β. (a) Heave motion on ship 1; (b) heave motion on ship 2; (c) roll motion on ship 1; (d) roll motion on ship 2; (e) pitch motion on ship 1 and (f) pitch motion on ship 2.

4.3. Effects of transversal distance between ships

Provided that other external conditions remain unchanged, different transverse distances between ships affect the wash wave propagations during the encountering of two ships. Fig. 16 displays the transient heave, roll and pitch motion responses of two ships during their encountering in the waves (β=180°) with three different transverse distances *dt* (*dt*=0.6 m, 1 m and 2 m). The motions of two ships during advancing are resulted from the combined action of the incident waves and the scattered waves of each ship as well as the scattered wave system of the other ship next to it. Fig. Fig. 17-Fig. 19 reflect the transient wave patterns during the three encounter states in the head wave at different transverse distances, which explains the effect of wave interference on the transient motions of two ships in Fig. 16 more clearly.

As shown in Fig. 16, at the wavelength λ = 3 m, the heave and pitch motions of ship 1, which is in head waves, are less sensitive to the changes in the transverse distance. This indicates that the wave propagation generated by ship 2 has a small effect on the heave and pitch motion of ship 1. From Fig. 16(b) and (f), it is obvious that the heave and pitch changes of ship 2. Before the two ships meet, the heave and pitch motions of ship 2 are almost unaffected by the transverse distance as ship 1. During the period from the beginning of the bow meeting to the complete departure of the stern, the increase of *dt* raises the propagation distance of the wave interference, and the frequencies of the heave and pitch oscillations of ship 2 interfered with the bow propagation of ship 1 decreases in the same period. Observing Fig. 16 (b) and (f), *dt* changes from 0.6 m to 1.0 m, the changing trend and amplitude size of the heave and pitch motion of ship 2 are not much different, this is due to the small change of *dt*, under these two values of *dt*, the action time of wave propagation generated by ship 1 to ship 2 is relatively close, as can be seen from Fig. Fig. 17-Fig. 19 (a) and (b), in the case of the two ships at the same longitudinal distance, the ship 2 receives the evanescent waves generated by ship 1 is approximately the same in extent. Fig. 16(c) and (d) show the transient roll motions of two ships. The increase in *dt* weakens the wave interference effects between two ships, making the amplitudes of the transient roll motions decrease for both ships and the peak transverse motions occur with a delay.

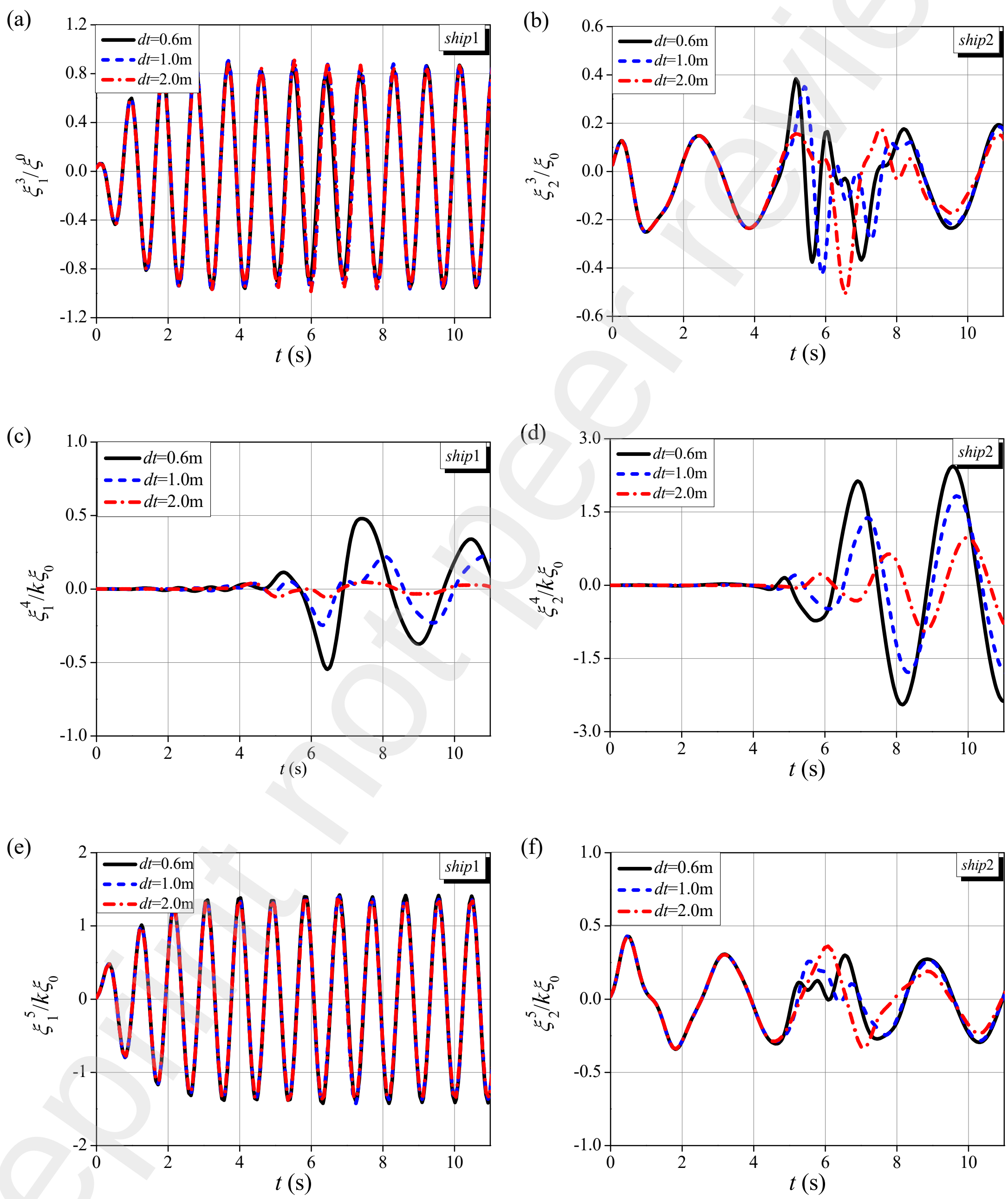

Fig. 16. Transient response of ship motions with various transverse distances. (a) Heave motion on ship 1; (b) heave motion on ship 2; (c) roll motion on ship 1; (d) roll motion on ship 2; (e) pitch motion on ship 1 and (f) pitch motion on ship 2.

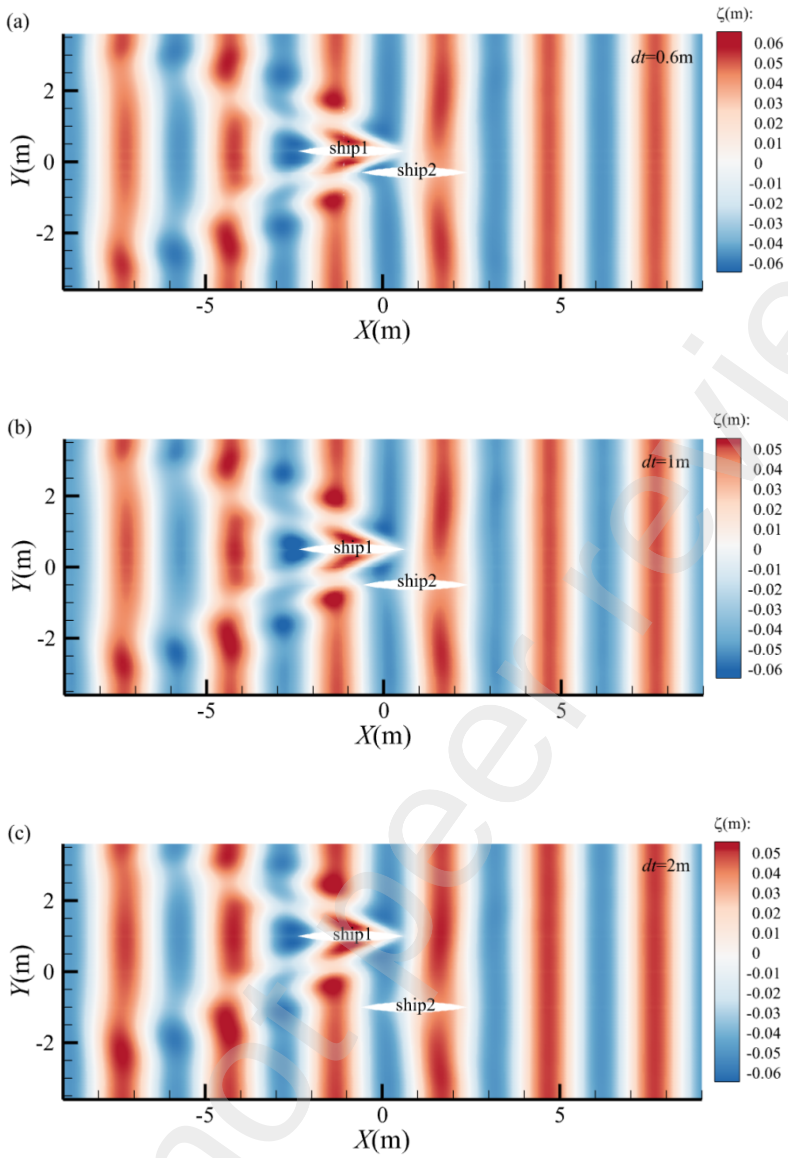

Fig. 17. Distribution of wave field around two ships when ships bow-encountering in an opposite direction with different transverse distances i.e. (a) *dt*=0.6m, (b) *dt*=1m, (c) *dt*=2m.

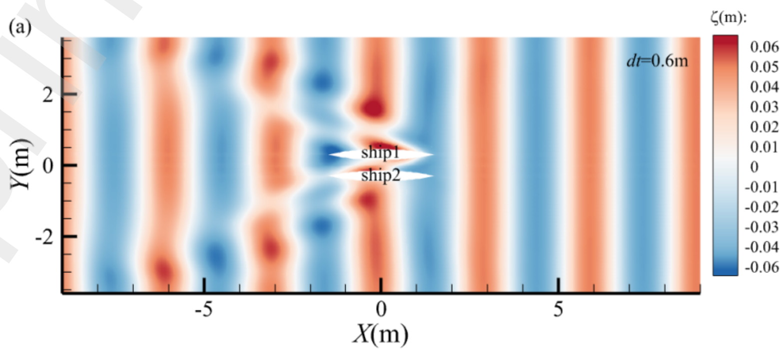

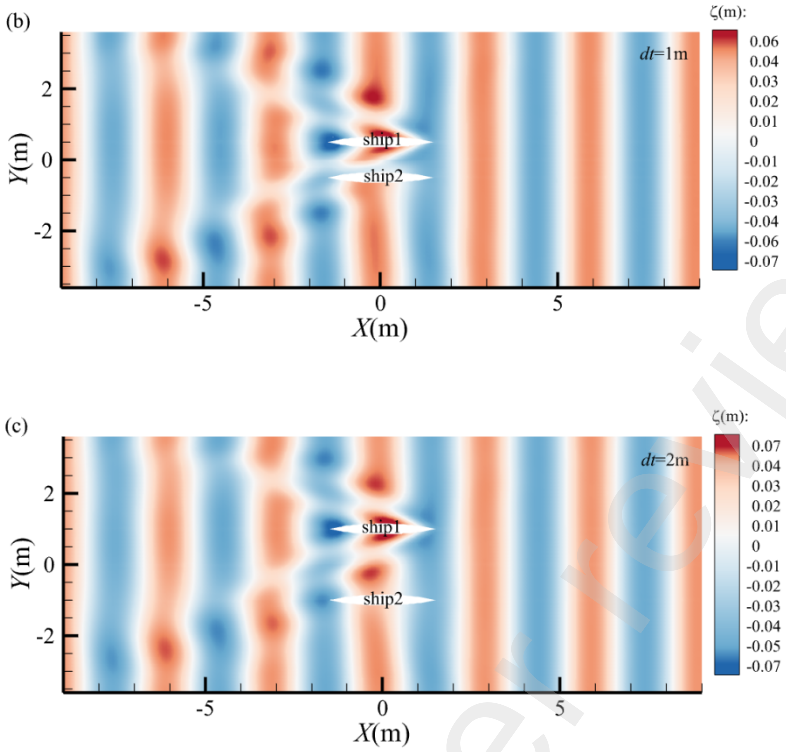

Fig. 18. Distribution of wave field around two ships when ships encountering in an opposite direction with different transverse distances i.e. (a) dt=0.6m, (b) dt=1m, (c) dt=2m.

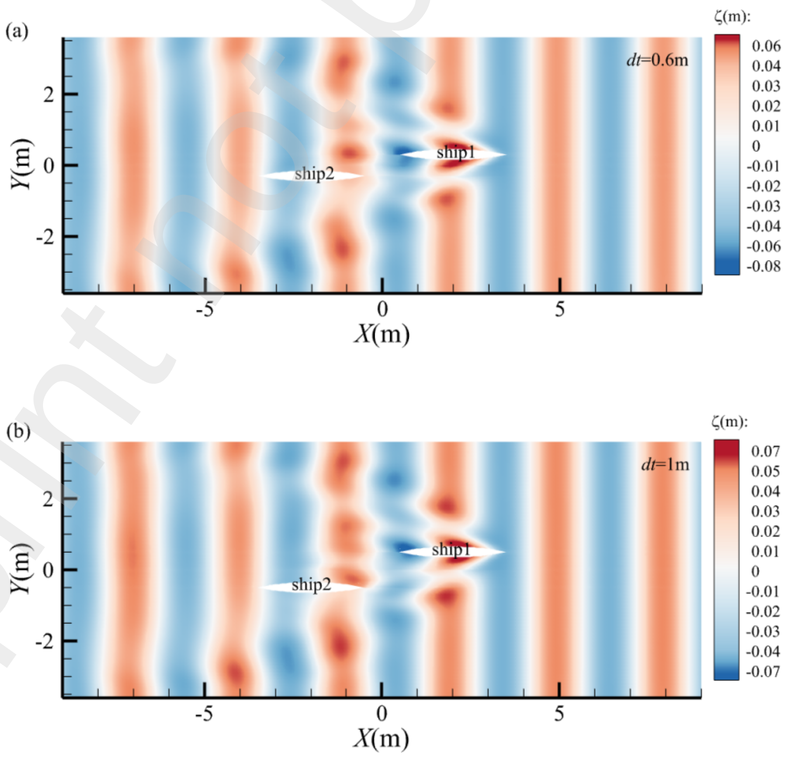

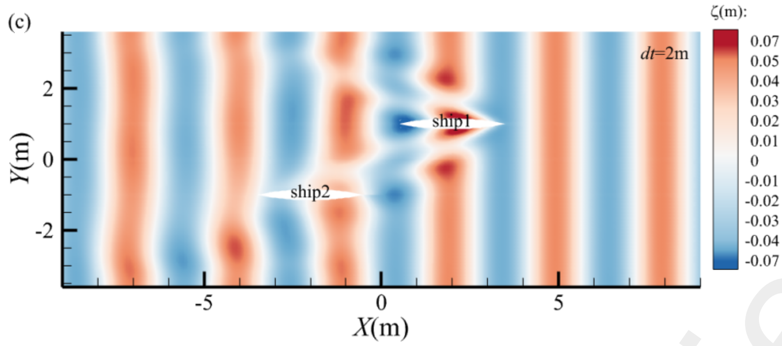

Fig. 19. Distribution of wave field around two ships when ships stern-encountering in an opposite direction with different transverse distances i.e. (a) *dt*=0.6m, (b) *dt*=1m, (c) *dt*=2m.

4.4. Effects of different ship sailing speed ratios

Fig. 20 compares the transient motions of two ships advancing in opposite directions in head wave at $\lambda = 1.0$m for different $|U_2/U_1|$ at the same time. At the same time, the speed of ship 1 remains constant and the encounter frequency ω_e of ship 2 gradually decreases as its own speed increases, which makes τ_2 ($\tau_2 = U_2/\omega_e g$) decrease and shortens the time needed for the response of ship 2. The attitude of the ship 2 motion changes, and the transient heave and pitch motions of ship 2 become smaller, at $|U_2/U_1| = 0.5$, the transient heave amplitude of ship 2 can reach 0.5, which decreases to less than 0.3 when $|U_2/U_1|$ increases. On the contrary, ship 1 is subjected to the action of ship 2 in its longitudinal direction, and its heave and pitch motions are slightly increased. Observing Fig. 20 (c) and (d), even though there is no change in the speed of ship 1, ship 1 is still subjected to diverging waves and transverse waves generated by ship 2 and the increase in the speed of ship 2 shortens the meeting time of two ships, so there is an increase in the amplitude and frequency of the roll motion of two ships in the same period.

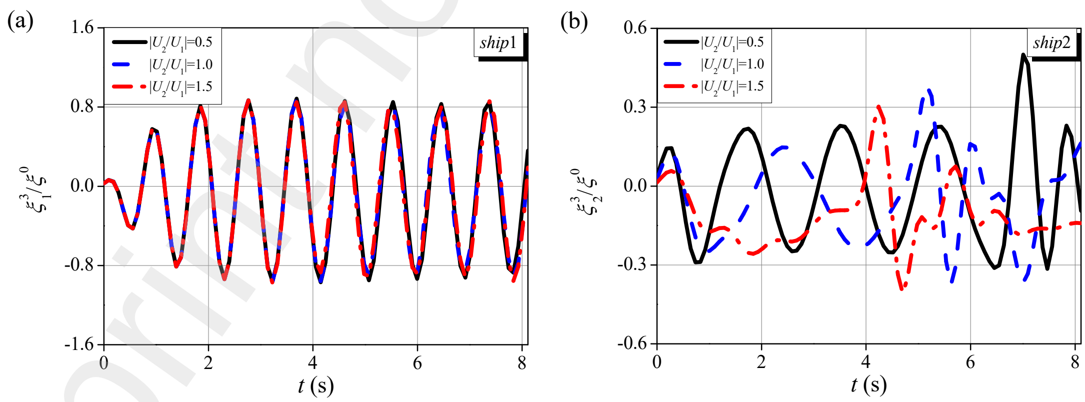

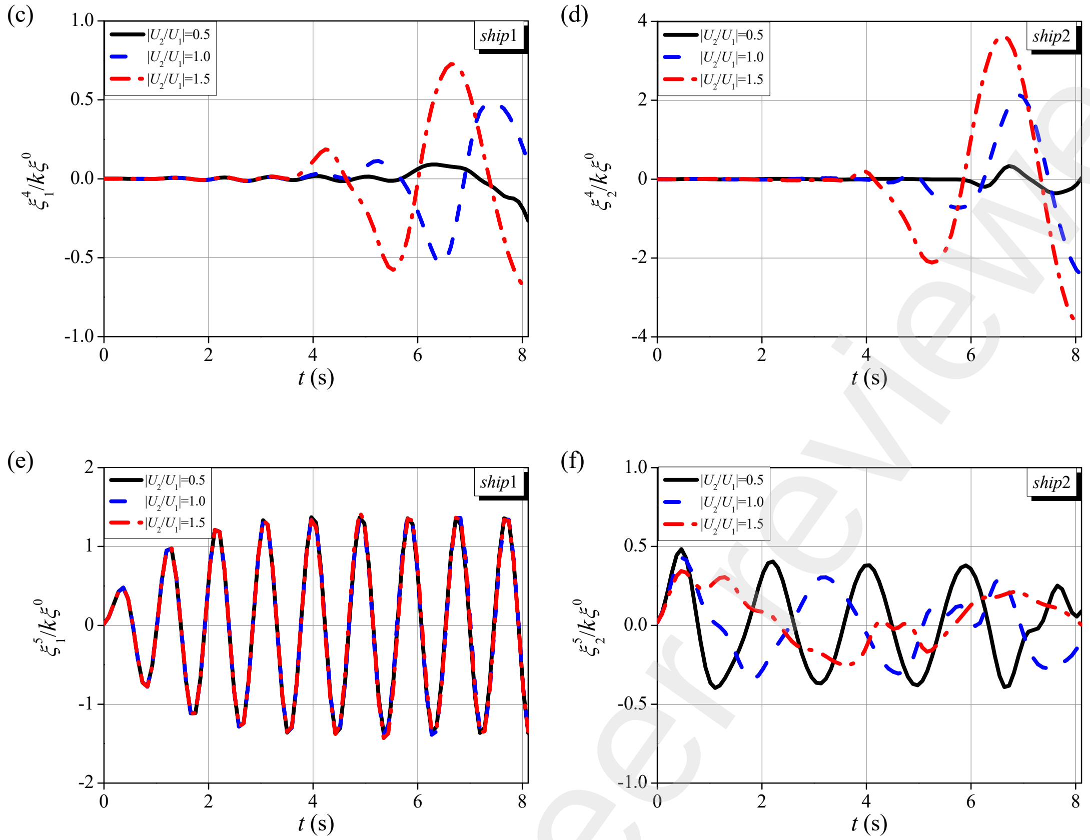

Fig. 20. Time series of ships' motions over different speed ratios. (a) Heave motion on ship 1; (b) heave motion on ship 2; (c) roll motion on ship 1; (d) roll motion on ship 2; (e) pitch motion on ship 1 and (f) pitch motion on ship 2.

5. Conclusion

A numerical model of two ships encountering in waves toward an opposite direction is developed based on the global coordinate system by applying the linear potential flow theory and the time-domain Rankine BEM. Two ships are decoupled by the superposition principle, considering linear free-surface boundary conditions separately, and the velocity potential and the free surface wave height at the next moment are predicted by the two-dimensional interpolation until the end of the computation. Since the whole process is dynamic, the computational grid distribution needs to be updated every moment following the movement of ships. This numerical computational procedure has been developed that can be applied to calculate and analyze instantaneous motions and wave field change generated by wave-structure interactions, and the following conclusions can be drawn:

(1) For ships advancing in waves, both the external wave environment and their own speeds affect the encounter frequency, which in turn affects the ships' navigational state and changes in motion. Compared to ships advancing in head waves, ships advancing in following waves are more susceptible to wave disturbances leading to unstable movements.

(2) The transient motion of the ship and the state of the flow field are related to the characteristics of incident waves. The propagation and reflection of scattered waves when two ships are advancing close together affects the instability of motions, and even if the ships move away from each other after approaching, they are still subjected to the effects of the wash waves

from the other ship. The effect of wave properties such as different wavelengths on the transient motion of the ship as well as the change of the wave field still needs to be further investigated.

(3) The transverse distance between ships not only affects the amplitude of the ships' heave, roll and pitch motions, but also changes the frequency of the roll motions of the two encountering ships. As the transverse distance increases, the transient response amplitude and amplitude oscillations of the ship is significantly smaller. Appropriately increasing the transverse distance between sailing ships to delay the arrival of ship-dispersed waves at ships could reduce wave interference.

(4) The transient motions of ships are sensitive to the velocity ratio between ships. An increase in the speed of the ship in the following waves causes an increase in the amplitude of the roll motion of a ship in head waves. The choices of a suitable transverse distance and the velocity ratio between ships need to be followed up with further exploration.

(5) When two ships pass through each other in waves, each ship is subject to lateral interference given by the other. The transient responses exhibit significant unstable behavior due to complex wave disturbances, such as sudden increases in the amplitude of motion and asymmetric motion, and such unstable characteristics are potentially risky for ship stability.

Hydrodynamic interactions between two or more ships are particularly complex in wave environments, and there are many influences to consider, with ship-to-ship advancing conditions prevalent in dense waterways. Through the motion simulation of ship-to-ship encounters in incident waves established based on the global coordinate system, the two ships advancing at different speeds resulting in different encounter frequencies and complex interference in the wave field, the analysis of the transient motion response of the ship and the changes in the wave field can capture the instantaneous behavior of the ship in the process of encountering, analyze the strength of the interference effect, and take targeted measures to reduce the impact of the transient response on the ship's stability. This study is based on linear theory, subsequently, the existing numerical models can be improved to increase the computational accuracy, and further study under nonlinear theory, sidewalls can be added to the existing models or to help predict the ship's response in extreme situations to avoid ship collisions.

CRediT authorship contribution statement

Xiao Zhang: Methodology, Validation, Formal analysis, Writing-original draft, Investigation. **Yong Cheng:** Data curation, Writing-original draft, Supervision. **Saishuai Dai:** Formal analysis, Data curation, Writing-review & editing, Supervision. **Mingxin Li:** Writing-review & editing, Supervision. **Zhiming Yuan:** Writing-review & editing. **Atilla Incecik:** Supervision.

Declaration of Competing Interest

The authors declare that they have no known competing financial interests or personal relationships that could have appeared to influence the work reported in this paper.

Acknowledgment

The authors are grateful to the National Natural Science Foundation of China (Grant No. 52271278, 52111530137), Natural Science Found of Jiangsu province (Grant No. SBK2022020579), Natural Science Found of Jiangsu province (Grant No. BK20241015) and the Newton Advanced Fellowships (Grant No. NAF\R1\180304) by the Royal Society for supporting this work.

References

[1] Vantorre, M., Verzhbitskaya, E., Laforce, E.J.S.T.R., 2008. Model test based formulations of ship-ship interaction forces. 49 (3), 124-141.

[2] Ohkusu, M.J.B.N., 1976. Ship Motions in Vicinity of a Structure.

[3] Kodan, N., 1984. The Motions of Adjacent Floating Structures in Oblique Waves. Journal of Energy Resources Technology 106 (2), 199-205. https://doi.org/10.1115/1.3231038 %J Journal of Energy Resources Technology.

[4] Ronæss, M., 2002. Wave induced motions of two ships advancing on parallel course.

[5] Korsmeyer, F.T., Lee, C.-H., Newman, J.N., 1993. Computation of Ship Interaction Forces in Restricted Waters. Journal of Ship Research 37 (04), 298-306. https://doi.org/10.5957/jsr.1993.37.4.298 %J Journal of Ship Research.

[6] Pinkster, J.A.J.I.s.p., 2004. THE INFLUENCE OF A FREE SURFACE ON PASSING SHIP EFFECTS. 51, 313-338.

[7] Yuan, Z.-M., Li, L., Yeung, R.W., 2019. Free-Surface Effects on Interaction of Multiple Ships Moving at Different Speeds. Journal of Ship Research 63 (4), 251-267. https://doi.org/10.5957/josr.10180089.

[8] Li, M.-X., Yuan, Z.-M., Tao, L., 2021. An iterative time-marching scheme for the investigation of hydrodynamic interaction between multi-ships during overtaking. Journal of Hydrodynamics 33 (3), 468-478. https://doi.org/10.1007/s42241-021-0051-7.

[9] Li, M., 2020. Steady and Unsteady Waves Generated by a Moving Body and Multiple Bodies.

[10] Yuan, Z.-M., Chen, M., Jia, L., Ji, C., Incecik, A., 2021. Wave-riding and wave-passing by ducklings in formation swimming. Journal of Fluid Mechanics 928. https://doi.org/10.1017/jfm.2021.820.

[11] Zhou, J., Ren, J., Bai, W., 2023. Survey on hydrodynamic analysis of ship-ship interaction during the past decade. Ocean Engineering 278. https://doi.org/10.1016/j.oceaneng.2023.114361.

[12] Yuan, Z., Incecik, A., 2016. Investigation of side wall and ship model interaction.

[13] Li, M.-x., Yuan, Z.-m., Bai, X., Li, Y.-z., Cheng, Y., Tao, L.-b., 2023. Numerical Modelling of Wash Waves Generated by Ships Moving over An Uneven Bottom. China Ocean Engineering 37 (1), 145-153. https://doi.org/10.1007/s13344-023-0012-8.

[14] Li, L., Yuan, Z., Gao, Y., 2018. Wash wave effects on ships moored in ports. Applied Ocean Research 77, 89-105. https://doi.org/10.1016/j.apor.2018.06.001.

[15] Kashiwagi, M., Endo, K., Yamaguchi, H., 2005. Wave drift forces and moments on two ships arranged side by side in waves. Ocean Engineering 32 (5-6), 529-555. https://doi.org/10.1016/j.oceaneng.2004.09.005.

[16] Zhu, R.-c., Miao, G.-p., Zhu, H.-r.J.J.o.H., 2006. The Radiation Problem of Multiple Structures with Small Gaps in Between. 18, 520-526.

[17] Yuan, Z.-M., 2014. Hydrodynamic interaction between ships travelling or stationary in shallow waters.

[18] Chen, X., Zhu, R.-c., Yang, Y.-t., 2018. Time-Domain Analysis of Motion Responses of Side-by-Side Vessels During Offshore Installations and Underway Replenishment. International Journal of Offshore and Polar Engineering 28 (01), 19-30. https://doi.org/10.17736/ijope.2018.jc711 %J International Journal of Offshore and Polar Engineering.

[19] Yong, -.X., Wen-cai, -.D., 2014. - Hydrodynamic Interactions Between Multiple Ships

Advancing Parallel in Close Proximity in Waves %J - Applied Mathematics and Mechanics. - 35 (- 4), - 389. https://doi.org/- 10.3879/j.issn.1000-0887.2014.04.005.

[20] Li, M., Pan, S., Cheng, Y., Yuan, Z.-M., Tao, L., 2023. Time-domain numerical simulation for multi-ships moving in waves with forward speed. Ocean Engineering 290. https://doi.org/10.1016/j.oceaneng.2023.116325.

[21] He, G., 2013. An iterative Rankine BEM for wave-making analysis of submerged and surface-piercing bodies in finite water depth. Journal of Hydrodynamics 25 (6), 839-847. https://doi.org/10.1016/s1001-6058(13)60431-x.

[22] Tang, K., Zhu, R.-c., Miao, G.-p., Fan, J., 2014. Domain decomposition and matching for time-domain analysis of motions of ships advancing in head sea. China Ocean Engineering 28 (4), 433-444. https://doi.org/10.1007/s13344-014-0035-2.

[23] Zhou, W.-j., Zhu, R.-c., Chen, X., Hong, L., 2020. Vertical integral method incoporated with multi-domain HOBEM for time domain calculation of hydrodynamics of forward speed SHIP. Applied Ocean Research 94. https://doi.org/10.1016/j.apor.2019.101997.

[24] Pan, S.-y., Cheng, Y., 2024. A Time-Domain Numerical Simulation for Free Motion Responses of Two Ships Advancing in Head Waves. China Ocean Engineering 38 (3), 519-530. https://doi.org/10.1007/s13344-024-0041-y.

[25] Journee, J.M.J., 1992. Experiments and calculations on Four Wigley Hullforms.